

Core-level binding-energy shifts during metal adsorption and compound formation: Yb/Ni(100)

A. Nilsson, B. Eriksson, and N. Mårtensson

Department of Physics, Uppsala University, Box 530, S-751 21 Uppsala, Sweden

J. N. Andersen* and J. Onsgaard

Institute of Physics, Odense University, Campusvej 55, DK-5230 Odense M, Denmark

(Received 15 April 1988)

A model for core-level shifts in metallic overlayers is introduced. The model is based on a decomposition of the shift into partial shifts which are related to specific structural aspects of the interface system. The model is applied to the Yb/Ni(100) overlayer system which has been studied by He II and Al $K\alpha$ excited photoelectron spectroscopy. The deposition of Yb is investigated at two substrate temperatures, room temperature and 670 K. At 670 K ordered low-energy electron diffraction structures are seen, and at higher Yb depositions intermixing with the substrate occurs. At room temperature no ordered structures are seen. The low mobility of the atoms furthermore prevents strong intermixing with the substrate. It is shown that an analysis of the divalent and trivalent Yb shifts provides detailed structural information about the Yb/Ni(100) overlayer system.

I. INTRODUCTION

One of the main reasons for the strong interest in photoelectron spectroscopy is that measurements of core-level binding energies and chemical shifts of these give information on the chemical state of the various atoms in a system.^{1,2} The original understanding of the chemical shift was based on charge transfer and electrostatic effects in the initial state. However, already at an early stage it was realized that one has also to consider how the system responds to the creation of the core hole.^{3,4} The final state effects are often difficult to account for, and it has therefore been common to totally neglect these. However, especially for metallic systems such an approach may lead to most misleading conclusions.

Based on the assumption of complete electronic screening,⁵⁻⁸ a model for chemical shifts has been developed which successfully describes the shift in many different situations.⁸ The shifts can be described in terms of various thermodynamical quantities. The model takes into account chemical changes both in the initial and final states. Using this approach, chemical shifts in many types of systems such as alloys,⁸⁻¹¹ surfaces (with and without adsorbed molecules,^{8,12-15} and interfaces¹⁶ have been successfully treated.

The application of photoelectron spectroscopy to surface related problems has been most successful due to the inherent surface sensitivity of the method. For adsorbate and interface systems the binding energies have mainly been used to identify different species or to follow the intermixing between an overlayer and the substrate. However, in some cases more detailed information on, e.g., the coverage dependence of the shifts has been obtained and discussed with consideration of both initial- and final-state effects.¹⁶⁻²³

The lanthanide metals are well suited for surface oriented photoemission studies since the localized 4f

electrons lead to sharp final-state multiplet structures. For some of the lanthanide metals also the 5p levels give rise to narrow spectral features. This makes it possible to extract small chemical shifts in the lanthanide spectra. Moreover, the 4f core-level positions are directly related to the stability of different valence states of the lanthanide metals (see e.g., Ref. 24).

In a series of papers we have presented a detailed study of the adsorption and interfacial properties of Yb on Ni(100). The structural aspects of this system have been discussed in two papers based on Auger electron spectroscopy (AES) ion-scattering spectroscopy (ISS), low-energy electron diffraction (LEED), and x-ray photoelectron spectroscopy (XPS) results.^{25,26} The deposition of Yb has been followed at two substrate temperatures, room temperature and 670-K. These temperatures represent different situations with respect to the mixing between Yb and the Ni (100) substrate. The main results from these papers can be summarized as follows.

Based on the variation of the substrate and overlayer AES intensities as a function of deposition time, three different regions for the 670-K depositions were defined. In region 1, an adsorbed divalent state at low coverages was seen which showed no ordered structure. For higher coverages, but still within region 1, an incommensurate structure was observed containing both divalent and trivalent Yb atoms. We denote this the ring 1 structure. At a threshold coverage of Yb an intermixing between Ni and Yb starts in region 2, giving rise to a $c(10 \times 2)$ LEED pattern. This was interpreted as due to the formation of a surface intermetallic compound. The heterogeneously mixed valent character of this compound has been discussed in a separate paper.²⁷ With further deposition the compound thickens leading in region 3 to trivalent Yb in the bulk and divalent Yb at the surface. The thick compound shows a slightly distorted hexagonal LEED pattern, with a complete absence of Ni(100) spots. We

denote this situation the "final structure." It was also noted that the unit cell of the final structure has a $c(10 \times 2)$ coincidence cell with the Ni(100) surface. For the room-temperature (RT) depositions it was found that the limited mobility of the surface atoms prevents the formation of ordered structures.

In the present paper further details of the Yb/Ni(100) interface will be discussed based on photoelectron results. The interface systems have been investigated both by ultraviolet photoelectron spectroscopy (UPS) and XPS. In particular, we have investigated the binding-energy shifts of Yb in the different situations. To guide the discussion a model is outlined for core-level shifts in overlayer systems. This model is based on a decomposition of the shift into partial shifts, which are related to specific structural aspects of the interface system.

II. EXPERIMENTAL

The experimental system consists of two interconnected ultrahigh vacuum (UHV) -chambers (base pressure 2×10^{-10} torr). The sample can be transferred between the sample manipulators in the two chambers by a transport system using magnetically coupled rods.

The first chamber is equipped with LEED optics, and a cylindrical mirror analyzer with an integral electron gun used for AES measurements.

The second chamber is used for high resolution XPS and UPS. The x-ray source consists of a high speed rotating anode and a 25-crystal monochromator on a Rowland circle arrangement. The uv- light is generated in a gas discharge lamp. To obtain pure He II α radiation a toroidal grating monochromator is used. This is important when studying deeper levels such as the Yb 5*p* level since the presence of He I radiation leads to large contributions to the spectra in the actual energy range. The electron spectrometer consists of a hemispherical analyzer with 36-cm mean radius and a multichannel detection system. The overall resolution in the present measurements was 0.1 eV and 0.4 eV for UPS and XPS, respectively.

The sample was heated by radiation from a tungsten filament on the manipulator and the temperature was measured with a Chromel-Alumel thermocouple spot-welded to the side of the crystal. The Ni(100) crystal was cleaned by a combination of Ar⁺ sputtering and annealing in vacuum or oxygen. The most persistent contamination was carbon which segregated from the bulk of the crystal. After prolonged periods of cleaning the carbon signal in AES was below the detection limit. High-purity Yb was evaporated from a tantalum foil by resistive heating. During evaporation the pressure never rose by more than 2×10^{-10} torr.

III. RESULTS

The growth of the Yb layers has been investigated both by UPS using He II radiation at 40.8 eV and by XPS at 1486.7 eV photon energy. The spectra obtained at these different energies have most different properties for the investigation of the Yb/Ni(100) overlayer systems. This is due to differences in the Yb-to-Ni cross-section ratios²⁸

as well as to differences in the probing depths. At 40.8 eV the cross-sections for the Ni 3*d* and Yb 4*f* states are of comparable magnitude. At XPS energies, on the other hand, the cross-section for the Yb 4*f* level is considerably larger than for the Ni 3*d* levels. At UPS energies the electron escape depth is very small. Especially it has been shown that an Yb overlayer leads to a very small escape depth in the energy range of 20–40 eV.²⁹ At these energies about half the signal originates from the outermost atomic layer. In XPS the escape depth is considerably larger and the intensity from the first atomic layer is in this case of the order of 15%.

The 4*f* emission of divalent Yb is characterized by a spin-orbit split doublet displaced by at most a few eV from the Fermi level. Trivalent Yb on the other hand gives rise to a more complex and several eV wide multiplet pattern at 5–16 eV binding energy. For low Yb coverages the 4*f* region can be difficult to utilize because the spectra are dominated by the overlapping Ni 3*d* intensity. Also the 5*p* spectra have been used to investigate the binding energy shifts and the valence state of Yb. In the 5*p* spectrum there is a shift of 2–3 eV between the divalent and trivalent configurations. In UPS only the divalent part of the 5*p*_{3/2} spectrum can be accurately used. The background is rapidly increasing at lower kinetic energies and the analysis of the trivalent 5*p* spectrum becomes very sensitive to the background subtraction procedure. Also the Ni 2*p* spectra were analyzed but no major changes in these spectra were seen.

The development of the spectra with deposition time for 670 K and at room temperature are summarized in Figs. 1–3. For each spectrum the Yb deposition time is indicated. The deposition times refer to the constant evaporation rate used in Ref. 26, and have in the present case been determined from the measured Yb-to-Ni Auger intensity ratios. For the 670 K depositions three regions were defined. The regions which were denoted 1, 2, and 3 correspond to deposition times of 0–6, 6–12, and > 12 min, respectively.

In Fig. 1(a) the UPS results obtained for different deposition times of Yb at 670 K are shown. The figure covers the valence-band region as well as the divalent part of the 5*p*_{3/2} spectrum. At the bottom of Fig. 1(a) the spectrum from a clean Ni(100) surface is shown as a reference. For a deposition time of 4 min a divalent feature is clearly seen in the 5*p* spectrum. In the valence-band (VB) region a weak 4*f* doublet is superimposed on the Ni VB spectrum. This corresponds to region 1 where an incommensurate structure is observed with LEED (denoted ring 1). At longer deposition times the spectrum changes drastically. In the spectrum obtained after 8-min deposition time (beginning of region 2) a second divalent feature at higher binding energy is seen. Simultaneously a trivalent feature becomes clearly visible in the 4*f* spectrum. The next spectrum shown in Fig. 1(a) is obtained after 12-min deposition time. In this spectrum only the high-binding-energy divalent feature is present. The shape of the trivalent spectrum undergoes a drastic change with the appearance of a second multiplet pattern. LEED shows in this region a $c(10 \times 2)$ pattern. In the spectrum obtained after 19 min deposition time (re-

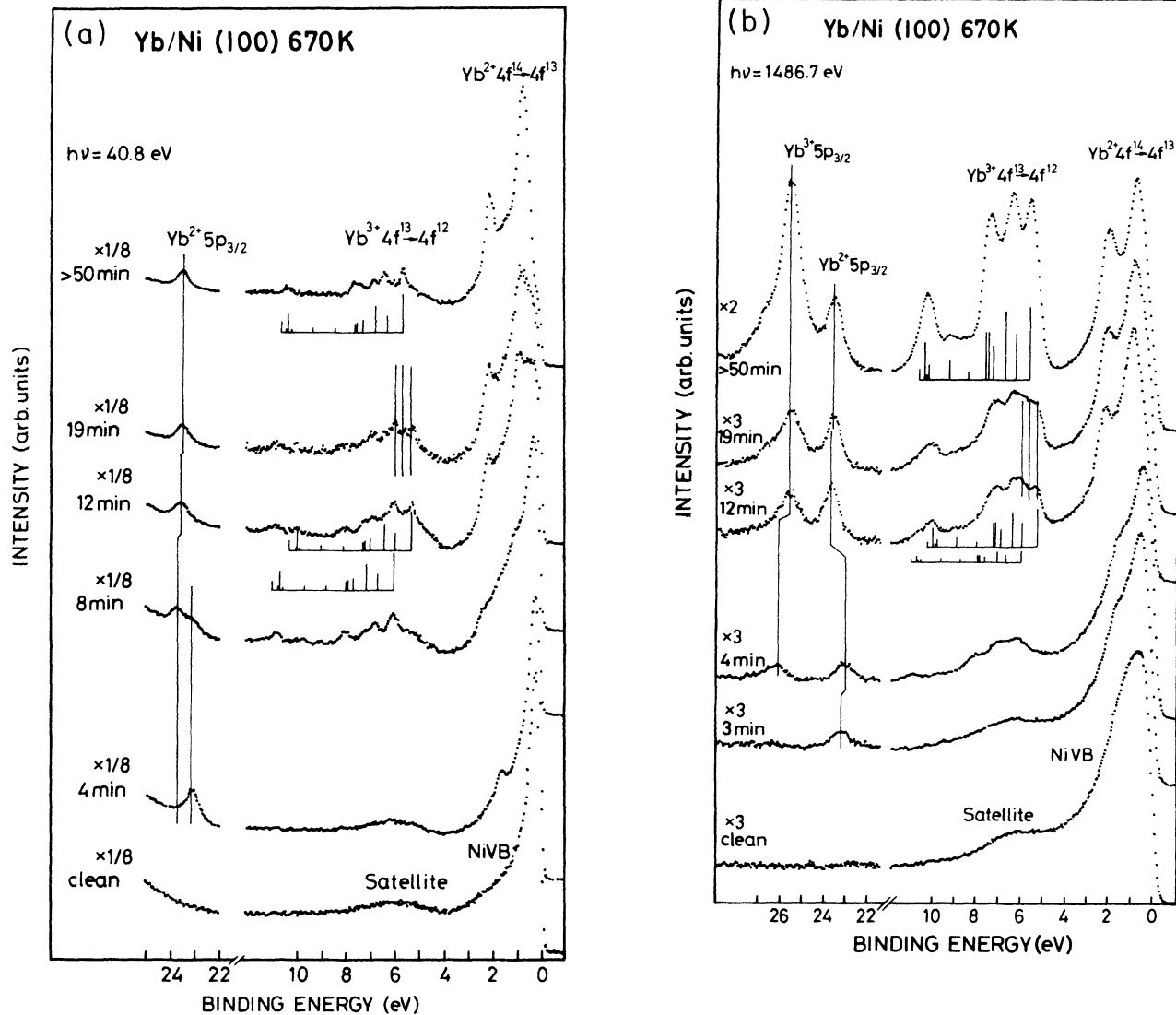


FIG. 1. UPS spectra of the $5p_{3/2}$ and valence regions for different Yb amounts deposited at 670 K. For the 12 min and > 50-min depositions a trivalent $4f$ multiplet pattern is indicated, see text. (b) XPS spectra of the $5p_{3/2}$ and valence regions for different Yb amounts deposited at 670 K. For the 12 min and > 50-min depositions a trivalent $4f$ fitted multiplet pattern is also included, see text.

gion 3) the divalent spectrum shows a small shift towards lower binding energy. In the trivalent spectrum a third multiplet pattern appears at a position between the two previous ones. For large depositions (> 50 min) this is the only remaining trivalent feature. This amount of Yb corresponds to a thick layer of the final intermetallic compound. Inspection of the $4f$ intensities shows that the divalent features give the most intense contribution to the spectrum also for the thick layer.

The variation of the shape of the divalent Yb $5p_{3/2}$ spectral feature obtained by UPS is illustrated in Fig. 2. The upper part of the figure shows two spectra for short deposition times which are all within region 1. The spectrum obtained after 1.5 min deposition time shows a line profile which is asymmetric towards higher binding energies. The full width at half maximum (FWHM) of this line is 0.78 eV. Increasing the Yb amount to 5-min deposition time, the line becomes significantly narrower

(FWHM of 0.52 eV). It is seen that the low-binding-energy side of the spectrum coincides with the preceding spectrum.

The lower part of Fig. 2 compares the widths of the spectra from regions 2 and 3. The 12-min spectrum has a FWHM of 0.65 eV. When the compound becomes thick (> 50 min) the spectrum narrows giving a FWHM of only 0.48 eV. It is furthermore seen that the narrowing occurs at the high-binding-energy side of the peak.

The development of the XPS spectrum for the 670 K depositions is shown in Fig. 1(b). The same trends in the binding energies are seen in XPS as in UPS. In the spectrum obtained after 3-min deposition time, the $5p$ spectrum shows only a divalent feature. Increasing the deposition time to 4 min leads to the appearance of trivalent Yb as seen from the $5p$ and the $4f$ spectra. The intensity of the trivalent features implies that some of the previously deposited Yb has been transformed to the trivalent

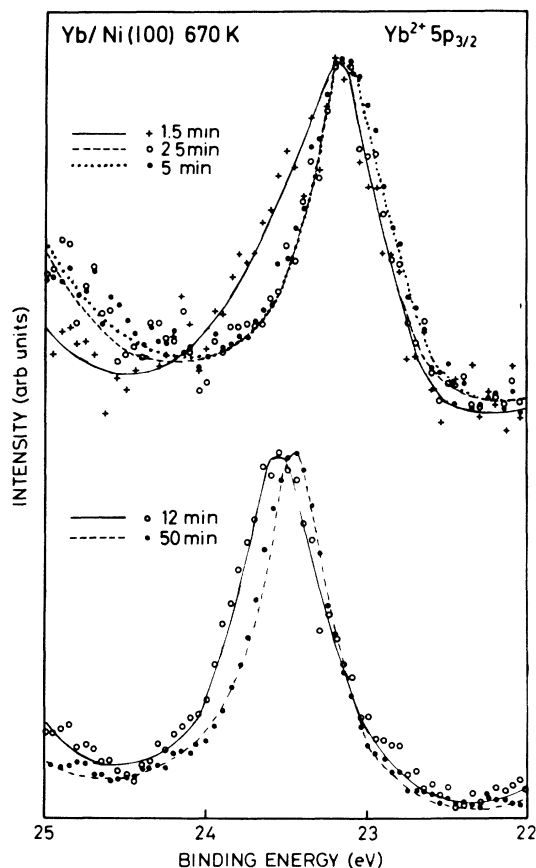


FIG. 2. HeII excited UPS spectra of the $\text{Yb}^{2+}5p_{3/2}$ level for different Yb amounts deposited at 670 K. The peaks are normalized to give the same peak height. The upper part of the figure represents region 1 and the lower part regions 2 and 3, see text.

state. From the $5p$ spectra it is concluded that equal amounts of divalent and trivalent Yb are present in the ring 1 structure. A small shift of the divalent peak to lower binding energy is also observed. In the spectrum obtained after 12 min deposition time (region 2), a shift of the trivalent feature to lower binding energies and a shift of the divalent feature to higher binding energies is seen. In the trivalent $4f$ spectrum an additional multiplet pattern appears at lower binding energy. This was also observed at higher resolution in the UPS spectra in Fig. 1(a). This explains the observed trivalent $5p$ shift and broadening. Based on the $5p$ intensities the ratio of trivalent to divalent Yb atoms was estimated to be 3:2. In the trivalent $4f$ spectrum the intensity of the low-binding-energy component is larger than the intensity of the high-binding-energy component. For 19-min deposition time no further shift of the trivalent $5p$ spectrum is observed. However, it is seen that the trivalent $4f$ spectrum becomes more featureless. As was seen in the UPS spectra in Fig. 1(a) this is due to the appearance of a third trivalent component between the two previous ones. In the spectrum for the thick compound both divalent and trivalent features are clearly seen. The trivalent features dominate and give rise to about 80% of the Yb intensity.

An analysis of the absolute intensities indicates that the divalent intensity has increased by 50% compared to the spectrum for 12-min deposition time.

The UPS spectra for the room-temperature depositions are shown in Fig. 3(a). A first difference compared to the 670 K spectra is that the features in the room temperature spectra are generally broader. At low coverages the spectra appear rather similar to the 670 K spectra. A divalent feature is seen at small deposition times. With increasing Yb deposition a shift of this feature to higher binding energies is observed. For large deposition times a typical spectrum for Yb metal appears with bulk and surface components shifted. The surface shift is large (0.65 eV) which indicates a disordered and poorly coordinated surface.³⁰

The room-temperature XPS spectra are shown in Fig. 3(b). At 1.5-min deposition time only a divalent feature is seen. At higher coverages also trivalent features appear both in the $5p$ and the $4f$ spectra. In the spectra obtained after 5- and 12-min deposition times the two valence states give rise to comparable intensities. The energy position of the trivalent $4f$ feature is the same as for the high-binding-energy component at 670 K. At 19-min deposition time, the spectrum has changed considerably. The divalent $5p$ spectrum shifts to higher binding energy, whereas the trivalent peak shifts to lower binding energy. With larger depositions the divalent feature becomes more prominent and there is a continuous decrease in the trivalent intensity. The trivalent position, however, remains approximately the same.

In order to analyze the details of the trivalent $4f$ spectra it is necessary to know the relative energies and intensities of the different multiplet lines. In XPS a well-defined trivalent spectrum is obtained after long deposition times. The trivalent $4f$ region of this spectrum is shown in Fig. 4 together with a fitted spectrum. The multiplet pattern for $\text{Tm}^{3+}(4f^{12})$ (Ref 31) is used as a basis and an expansion of 6.5% is required to reproduce the present Yb spectrum.³²

IV. MODEL FOR THE CHEMICAL SHIFT

In order to establish a connection between the core-level energies in overlayer systems and relevant structural parameters we formulate in this section an expression for the chemical shift which contains separate contributions due to alloying, surface effects, etc. This expression provides a method to obtain information concerning the surface and subsurface properties of the investigated system based on the measured shifts. The derivation is based on a previous treatment of core-level binding energies in metallic systems.⁸ Note that we use the term chemical shift for the complete shift in contrast to some authors who use this term to denote the initial-state orbital shift only.

The binding energy of a core electron is given by the total energy difference between the initial state and the core-ionized final state. Basic to our treatment is that the core-hole state is considered to be totally screened by the conduction electrons. This assumption has been well established for metallic systems. The core-hole state is

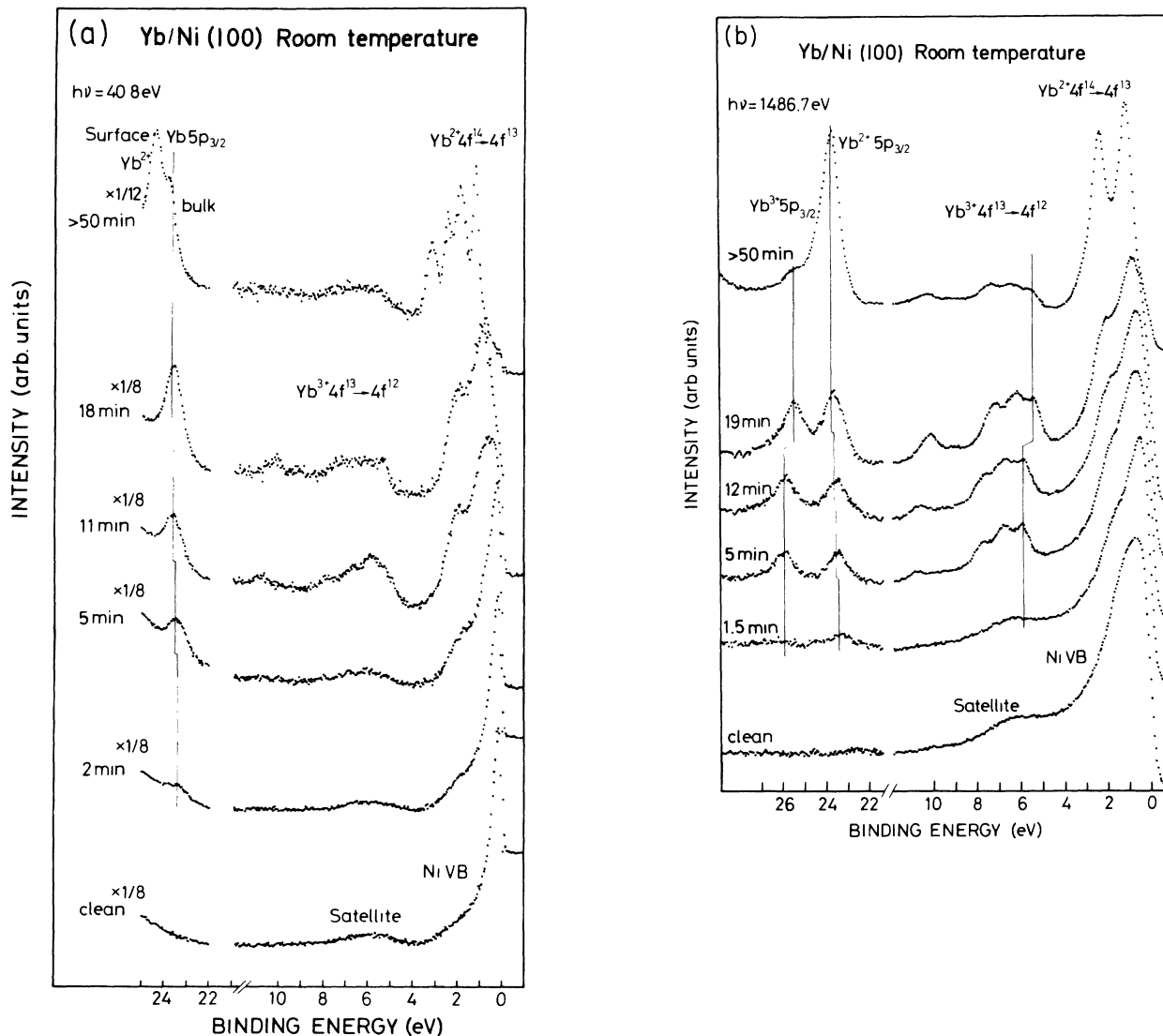


FIG. 3. (a) UPS spectra of the $5p_{3/2}$ and valence regions for different Yb amounts deposited at RT. (b) XPS spectra of the $5p_{3/2}$ and valence regions for different Yb amounts deposited at RT.

treated as a neutral Z^* impurity in the initial state metallic system.⁸ Z^* denotes a Z -metal atom with one core electron removed and one valence electron added. As an example let us consider the $4f$ ionization energy in divalent Yb, which has a $4f^{14}[5d6s]^2$ configuration. The brackets denote that the $5d6s$ valence electrons are in the metallic state. A $4f$ ionization of such an atom leads to the creation of a $4f^{13}[5d6s]^3$ site instead, i.e., Z^* is a trivalent Yb site. The measured $4f$ ionization energy is in this way directly related to the stability difference between the divalent and trivalent valence states of the lanthanide metal. In an analogous way the $4f$ ionization of a trivalent lanthanide leads to a tetravalent final-state impurity site. Although not essential to the present treatment, it can furthermore be noted that the valence electron properties of the Z^* atom in the general case to a good approximation resembles the properties of the $Z + 1$ element.⁸

In order to obtain an expression for the core-level binding energy in a general overlayer system we apply a Born-Haber cycle for the ionization process. The requirement on this expression is that it contains as explicitly as possible relevant structural parameters. We do this by separating the shift in terms of partial contributions due to the various atomic species in the system. To account for the surface effects we consider formally also vacuum as an alloying element. The shift expression is then obtained by weighting these partial contributions according to some effective structural parameters which describe to what extent each type of neighbor influences the ionized atom. If the partial shifts are known, the observed shifts can in this way be traced back to variations in the structural parameters, and information about the overlayer system can be obtained.

To start with we consider a core ionization in the pure Z metal. A Born-Haber cycle for this situation is shown

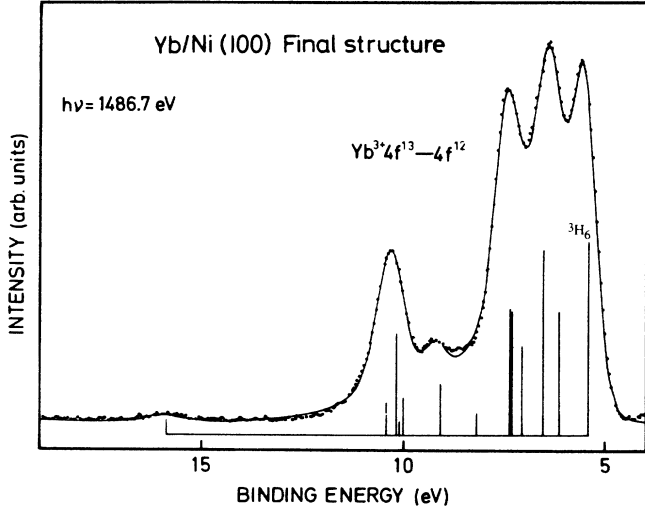


FIG. 4. Trivalent 4*f* region of the > 50-min deposition. The solid line represents the fitted spectrum and the bars the intensities and the positions for the fitted multiplet lines, see text.

in Fig. 5. Starting from the initial-state *Z* metal, we transform one of these atoms into a *Z** metallic atom and bring it to the bulk of a macroscopic piece of the hypothetical *Z** metal. This defines an energy E_B^0 . As can be seen this is the energy per atom which is required to transform a macroscopic number of *Z* atoms in the metallic state into a *Z** metal. As will be seen below, E_B^0 is a suitable reference binding energy for the discussion of chemical shifts in metallic systems. To reach the appropriate final state for the photoionization process in the metal *Z* we have to dissolve one of the *Z** metal atoms into the *Z* solid. This process defines the solution energy, $E_{\text{sol}}^{Z^*}(Z)$, of a *Z** impurity in the *Z* solid. The Born-Haber cycle is then closed by the core-ionization energy, $E_B^Z(Z)$;

$$E_B^Z(Z) = E_B^0 + E_{\text{sol}}^{Z^*}(Z). \quad (1)$$

Based on Eq. (1) we define the generalized shift ΔE_Z as

$$\Delta E_Z = E_B^Z(Z) - E_B^0 = E_{\text{sol}}^{Z^*}(Z). \quad (2)$$

We call this a generalized shift since it does not refer to a shift between two levels which can be measured by photo-

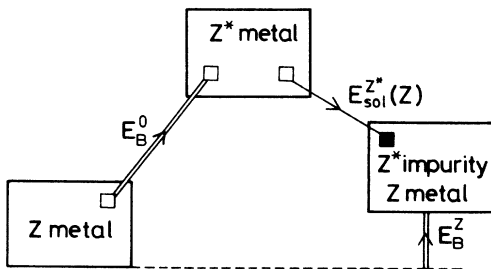


FIG. 5. Born-Haber cycle for the core ionization of a *Z* atom in a pure *Z* metal. The figure shows the relationship between E_B^Z , E_B^0 , and $E_{\text{sol}}^{Z^*}(Z)$.

emission but to the difference between a core-level position and the reference energy E_B^0 .

Next, we consider in the same way the alloying partial shift, ΔE_M , which accounts for the presence of *M*-metal neighbors around the core-ionized *Z* atom. In Fig. 6 a Born-Haber cycle for the case of a *Z* atom, completely surrounded by the *M* metal, is shown. As a first step in this cycle we bring a *Z*-impurity atom from the *M* metal into the metal *Z*. This defines the solution energy $E_{\text{sol}}^Z(M)$. Next we transform one of these *Z*-metal atoms to a *Z** atom and bring this one into the bulk of a *Z** metal. This requires again an energy E_B^0 . To reach the photoemission final state we have to bring one *Z** atom from the *Z** solid into the *M* metal releasing the solution energy $E_{\text{sol}}^{Z^*}(M)$ of a *Z** impurity in the *M* metal. This defines the core-level binding energy of the *Z*-metal impurity in *M* as

$$E_B^Z(M) = E_B^0 - E_{\text{sol}}^Z(M) + E_{\text{sol}}^{Z^*}(M), \quad (3)$$

$$\Delta E_M = E_B^Z(M) - E_B^0 = E_{\text{sol}}^{Z^*}(M) - E_{\text{sol}}^Z(M). \quad (4)$$

Lastly, we treat the effect of a reduced atomic coordination of the core-ionized atom. Such a situation is met at the surface. To include this in the same way as for the other types of neighbors, we treat formally this influence as an effect of alloying with vacuum. In analogy with the derivation of the other partial shifts we first consider a photoionization of a *Z*-metal atom which is completely surrounded by vacuum. Note that this is a purely hypothetical situation since we still consider the core-ionized site to be completely screened by a conduction electron from the surroundings (which of course requires interaction with the neighboring atoms). The partial shift ΔE_V is thus the shift that would be experienced as a consequence of a total loss of coordination. A Born-Haber cycle for this situation is presented in Fig. 7. Bringing together a macroscopic number of *Z* atoms defines the cohesive energy of the metal, E_{coh}^Z . Transforming one of these *Z*-metal atoms into a *Z** atom and bringing this into the bulk of the *Z** solid again requires

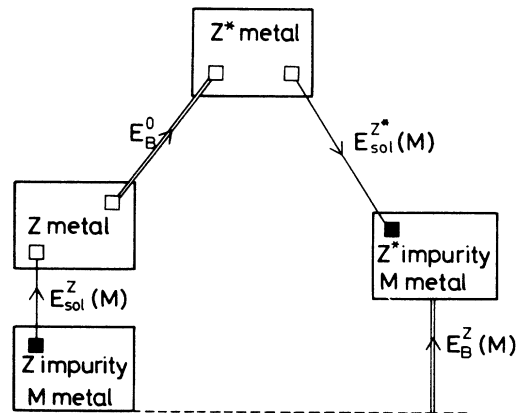


FIG. 6. Born-Haber cycle for the core ionization of a *Z* atom surrounded by an *M* metal. The figure shows the relationship between $E_B^Z(M)$, E_B^0 , $E_{\text{sol}}^Z(M)$, and $E_{\text{sol}}^{Z^*}(M)$.

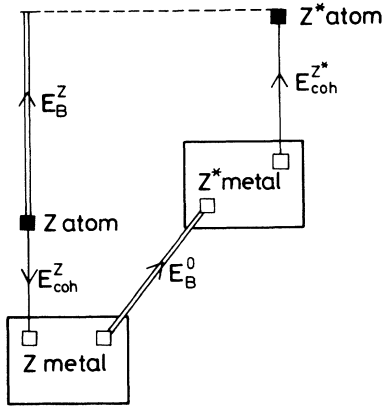


FIG. 7. Born-Haber cycle for the core ionization of a free Z atom. The figure shows the relation between E_B^Z , E_B^0 , E_{coh}^Z and $E_{\text{coh}}^{Z^*}$.

the reference binding energy, E_B^0 . In the next step we bring one of these Z^* atoms out of the solid, thereby defining the cohesive energy of the Z^* solid, $E_{\text{coh}}^{Z^*}$. In this way we obtain

$$E_B^Z(Z) = E_B^0 - E_{\text{coh}}^Z + E_{\text{coh}}^{Z^*}, \quad (5)$$

$$\Delta E_V = E_B^Z(V) = E_B^0 = E_{\text{coh}}^{Z^*} - E_{\text{coh}}^Z. \quad (6)$$

After having treated these basic situations we are now prepared to formulate an expression for a more general case. The shift is mainly influenced by the first coordination shells of the ionized atom. We therefore define a number of effective concentration parameters, c_Z^* , c_M^* , and c_V^* , which quantify the presence of the different kinds of neighbors around the ionized atom. The shift in the general situation is obtained as a weighted average of the partial shifts with these effective parameters as weight factors. We then obtain the following expression for the binding energy, E_B^Z , in the general situation;

$$E_B^Z = E_B^0 + c_Z^* \Delta E_Z + c_M^* \Delta E_M + c_V^* \Delta E_V. \quad (7)$$

It is important to note that c_Z^* , c_M^* , and c_V^* are effective parameters, and that their detailed relationships to the structure can be quite complicated. However, to a reasonable approximation they can be expected to depend on the structure in a rather straightforward way. It should also be noted that the effective character of the concentration parameters means that one cannot necessarily expect the sum of these to be equal to one.

To clarify the meaning of the concentration parameters we first consider the parameter, c_Z^* , which quantifies the effective number of Z -metal neighbors which the core-ionized Z -atom site experiences. Figure 5 corresponds to $c_Z^* = 1$. In a broken-bond model with only nearest-neighbor interaction c_Z^* is directly related to the number of Z neighbors of the core-ionized atom. If also next-nearest-neighbor interaction, etc., is included c_Z^* will instead denote a weighted average over the important coordination shells. In a model like Miedema's model^{33,34} which is based on interactions over the contact surface between different atoms, c_Z^* would instead denote the

fraction of the total contact surface of the ionized atom which is taken up by neighboring Z -metal atoms.

The c_M^* concentration parameter quantifies the effective number of the alloying M -metal neighbors of the core-ionized Z -atom site. Figure 6 corresponds to $c_M^* = 1$. The exact value of the c_M^* parameter will depend strongly on the local structure of the Z - M alloy in the vicinity of the ionized Z atom. In a fully disordered solid, the average value of c_M^* is expected to be rather similar to the concentration of the M metal or at least directly related to this concentration. In an ordered alloy, c_M^* will be larger than if the alloy is disordered. If there are Z sites which differ with respect to the number of neighboring M atoms, these sites will have different c_M^* values.

The c_V^* concentration parameter quantifies the lack of coordination of the core-ionized site. Figure 7 corresponds to $c_V^* = 1$. An atom at the surface of a metal will have a lower coordination than a bulk atom. It is a reasonable first approximation to simply count the number of missing nearest-neighbor atoms when calculating c_V^* . However, for a more refined analysis it is necessary to include the detailed surface structure. A more open surface naturally corresponds to a larger effective c_V^* value. A surface reconstruction, on the other hand, is expected to have a tendency to reduce c_V^* . Furthermore, it seems that there are also significant differences between close-packed fcc and bcc surfaces even if the number of nearest neighbors is rather similar.³⁵

The expression in Eq. (7) can be generalized to more types of atoms in the system by including more terms of the same kind as in Eq. (3). In fact, in the present case we meet such a situation since Yb^{2+} and Yb^{3+} have significantly different chemical properties and must be treated separately.

Note also that Eq. (7) is based on the assumption that all partial shifts are additive. In a more strict analysis we would have to take into account that the different partial shifts themselves are functions of the different effective concentrations.

V. APPLICATION OF THE SHIFT MODEL TO THE Yb/Ni SYSTEM

In this section the model presented in Sec. IV will be used to discuss the expected trends of the binding energies in the Yb/Ni(100) overlayer system for different illustrative situations. Based on estimations of the partial shifts it is possible to get an impression of what shifts are expected for different structural changes in the overlayer system. In Fig. 8 the general trends of the divalent Yb $4f$ binding energies in the Yb/Ni system according to Eq. (7) are summarized. The contributions from the different partial shifts are shown approximately to scale.

The reference energy, E_B^0 , for the $4f$ level in divalent Yb represents the stability of the divalent configuration relative to a transition to the hypothetically trivalent state. This energy has been estimated to be 0.5 eV in the case of Yb.³⁶ This refers to a transition to the trivalent state of the whole Yb lattice. In the photoionization process, however, only one site is transferred to the trivalent state. Using the measured $4f$ binding energy which is

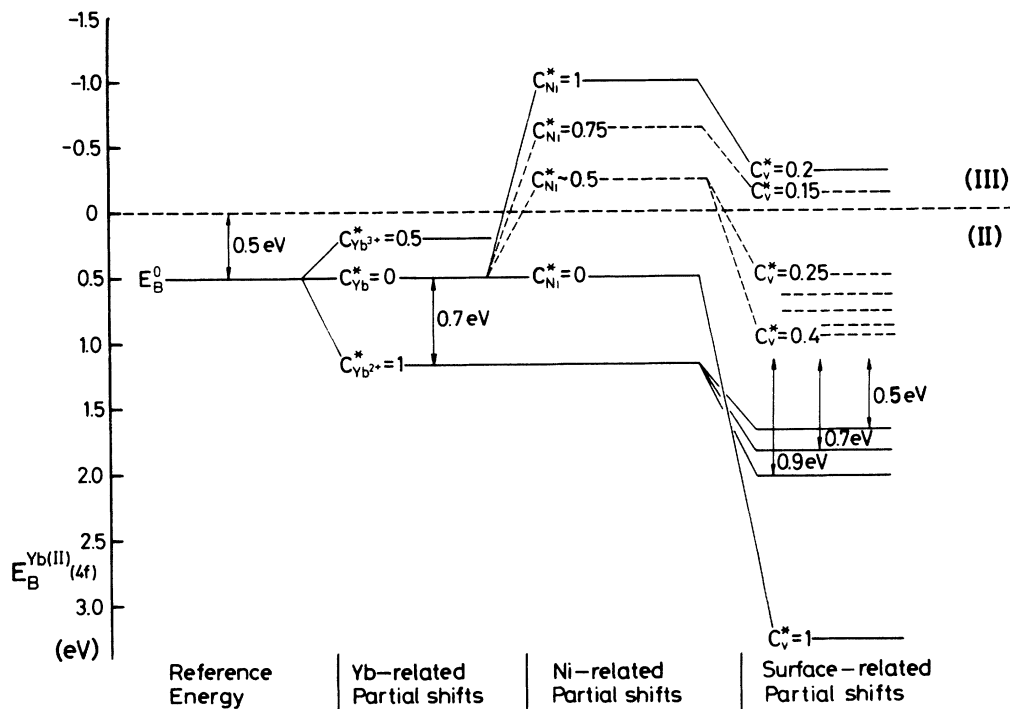


FIG. 8. Illustration of typical divalent Yb 4f shifts, see text.

1.17 eV this yields according to Eq. (1) a value of ≈ 0.7 eV for the $E_{Z^*}(Yb^{2+})$ term. It should be noted that when deriving the value for ΔE_{Z^*} in this way it will contain other effects than purely chemical ones. In the photoionization process there is no time for relaxation of the lattice. The final-state trivalent site is thus created with the geometry of a divalent Yb atom. This implies that the ΔE_{Z^*} solution energy is a restricted energy in the sense that it refers to the solution of a Z^* impurity with the atomic size of the original Z -metal atom. The thermodynamical solution energy, on the other hand, refers to an adiabatic situation with full lattice relaxation. This difference is, in general, very small, and it is in those cases not necessary to distinguish between the two types of solution energies. In the case of a photoionization of a divalent lanthanide atom, however, the size difference between the initial-state and final-state atoms is substantial. In this particular case the difference between the restricted and the adiabatic solution energies may amount to several tenths of an eV. The restricted solution energy included in Fig. 8, is, however, the appropriate quantity for discussing the 4f core-level position.

The shift of the bulk Yb 4f level as a function of Ni coordination can be estimated using experimental or calculated heat of formation data for the Yb-Ni system. Using solution energies, calculated by Miedema's scheme^{33,34} the characteristic energy shift, ΔE_M , for Yb in Ni can be estimated to be -1.5 eV. There exist five bulk YbNi intermetallic compounds; YbNi, YbNi₂, YbNi₃, YbNi₅, and Yb₂Ni₁₇.³⁷ All the bulk intermetallic compounds will therefore correspond to rather large c_M^* values. Due to the ordering in these compounds, all of

these will correspond to c_{Ni}^* values larger than 0.5 in the bulk. In Fig. 8 the 4f energy is included for $c_{Ni}^* = 0.5, 0.75$, and 1.0. As can be seen, all these compounds correspond to negative 4f energies, which implies that the trivalent configuration is more stable than the divalent configuration (the energy positions for the trivalent 4f configurations will be discussed below). This explains why all existing YbNi_x compounds are trivalent.³⁷ For the compounds with the highest Ni contents (YbNi₅ and Yb₂Ni₁₇) each Yb atom is completely surrounded by Ni atoms in the first coordination shell. This implies that c_M^* is close to 1 in these cases, leading to a stability of the trivalent state of as much as around 1 eV.

The shifts due to differences in atomic coordination can be substantial for a divalent lanthanide atom. Using Eq. (6) we obtain $\Delta E_V = 2.8$ eV for the divalent lanthanide metals. The difficulty is to estimate reasonable values of c_V^* for different situations. This means that it can be difficult to calculate absolute surface core-level positions. It is, however, more important that Eqs. (6) and (7) provide a means to relate observed trends in the binding energies with structural changes at the surface.

At first we show in Fig. 8 the magnitude of the shift for a complete loss of coordination ($c_V^* = 1$). As can be seen from the figure the stability of the divalent configuration in an isolated Yb atom is 3.3 eV. The reduction of this stability in the metal is due to the larger gain in cohesive energy of the trivalent configuration.

For the surface in the pure Yb metal a larger binding energy is observed than in the bulk. This shift has been measured for different atomic coordinations at the surface.³⁰ For a highly coordinated surface the shift is 0.5

eV. It was also seen that the shift becomes larger for surface atoms with lower atomic coordination. In the diagram the different experimental surface 4*f* binding energies from Ref. 30 are included. These were ascribed to Yb surface atoms with coordination numbers 7, 8, and 9, respectively. However, we have not specified what values of c_V^* these correspond to. A reasonable choice in many situations for a highly coordinated surface seems to be the value of 0.2 which was used in Ref. 8 when treating surface core-level shifts in the pure metals. Using this value of c_V^* and experimental values for the surface energies of liquid metals, good description of the surface core-level shifts in the 5*d* transition metals was obtained. For an isolated Yb atom adsorbed on a surface, there would be a much higher concentration of vacuum compared to having the atom in the surface plane.

In Fig. 8 we have for a compound with $c_{Ni}^* = 1$ in the bulk indicated the effect of introducing a surface. We then use $c_V^* = 0.2$. It is important to notice that the reduced coordination at the surface will also lead to a reduction of c_{Ni}^* . To a first approximation we assume that this parameter is reduced by the same factor of 0.2. With this choice of parameters it is seen that the surface 4*f* position is still located on the trivalent side in the diagram. In this connection it is interesting to note that in an XPS investigation of YbNi₅ no trace of divalent Yb was seen in the spectra,³⁸ indicating that the surface of this compound is indeed trivalent.

If we instead consider a situation with a smaller initial coordination to Ni (see, e.g., the situation with $c_{Ni}^* = 0.5$)

it is seen that already for a rather small c_V^* the surface becomes divalent. The position of the surface 4*f* level as seen with photoemission then depends on the magnitude of c_V^* , i.e., the coordination of the surface atom. For a less coordinated atom a larger binding energy will be seen, whereas a larger coordination leads to a 4*f*-level position closer to the Fermi level.

From this discussion it is evident that the surface of a Yb-Ni compound can be either divalent or trivalent depending on the composition and structure of the surface. However, from the fact that all bulk YbNi_x compounds are trivalent³⁷ it is also clear that if a divalent signal is seen it must be due to the surface.

Figure 9 shows a diagram for the trivalent 4*f* positions. E_B^0 has in this case been estimated to be 5.69 eV.³⁹ This represents the stability of the trivalent state relative to a transition to the tetravalent state. Next, the shift due to coordination to other Yb atoms is included in the diagram. The effect of surrounding Yb³⁺ atoms can be estimated from the experimental 4*f* positions in the trivalent lanthanide metals.⁴⁰ By studying the difference between E_B^0 and the spectroscopic 4*f* positions in a number of trivalent lanthanide metals it is seen that a value of -0.15 eV is obtained for $E_{sol}^{Z*}(Z)$ according to Eq. (1).²⁴ The sign of $E_{sol}^{Z*}(Z)$ obtained in this way is consistent with the fact that trivalent and tetravalent metals form solid solutions. There may also be situations in which a trivalent Yb atom is surrounded by divalent Yb atoms. Using Miedema's scheme^{33,34} for the solution energies in Eq. (4) for $M = Yb^{2+}$ a $\Delta E_{Yb^{2+}}$ shift of 0.8 eV is ob-

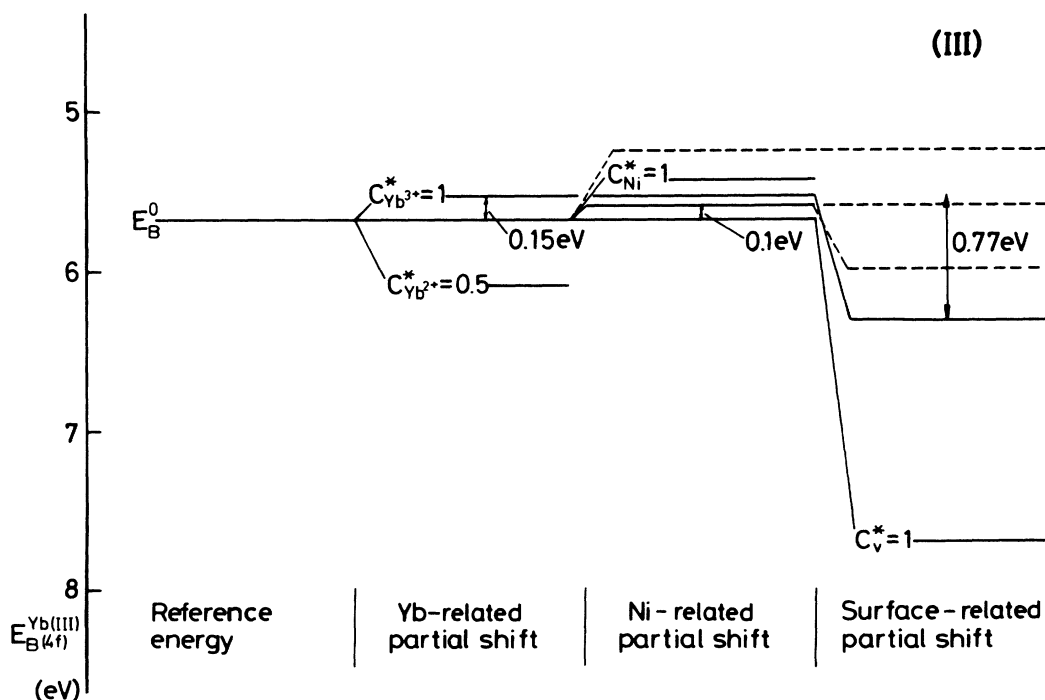


FIG. 9. Illustration of typical trivalent Yb 4*f* shifts, see text.

tained. In Fig. 9 the effect of this shift is included for an effective concentration parameter, $c_{\text{Yb}^{2+}}^*$, of 0.5.

In the next step in Fig. 9 the effect of Ni neighbors is considered. We have estimated this effect in several ways. First of all we have included the experimental position for YbNi_5 .³⁸ This binding energy furthermore agrees with the one obtained in the present investigation for the thick reacted films. This defines a shift of 0.1 eV to lower binding energy relative to E_B^0 for Yb^{3+} in Ni. We have also estimated the shift in Eq. (4) using solution energies according to Miedema's scheme.^{33,34} A ΔE_{Ni} shift of -0.27 eV is obtained in this way.

The effect of introducing a surface is substantial also for a trivalent lanthanide metal. For the trivalent metal Lu, which is the neighboring element of Yb in the Periodic Table, a surface shift 0.77 eV has been determined.⁴¹ This should, to a good approximation, be the shift also for the hypothetical Yb^{3+} metal. This surface shift is included in Fig. 9 as the shift between the expected experimental position for the bulk of trivalent Yb metal and the expected position for the surface of trivalent Yb. According to Eq. (6) a ΔE_V shift of 2.01 eV is obtained for a complete loss of coordination ($c_V^* = 1$).

The dashed lines to the right in the figure represent the measured positions in the Yb/Ni(100) overlayer system. These positions will be discussed in more detail below.

VI. DISCUSSION

A. Binding energies—670 K

The development of the binding energies with Yb deposition time at 670 K is summarized in Fig. 10. Both the UPS and XPS results are included in the figure. There are slight differences between the XPS and UPS energies, but these deviations are within the error limits for the calibration of the energy scales. The errors in the determination of the AES intensity ratios may also introduce some uncertainties. However, the trends in the binding energies agree well between the two sets of results. From this comparison it can be concluded that the relative shifts are determined with an accuracy of about 0.05 eV.

The binding energies in Fig. 10 refer to the $(4f^{13})^2F_{7/2}$ level for divalent Yb and the $(4f^{12})^3H_6$ level for trivalent Yb, respectively. For divalent Yb it is in some cases most practical to perform the shift determinations for the $5p_{3/2}$ level. It is then simply assumed that the $5p$ and $4f$ shifts are the same. This procedure is not expected to add significantly to the errors in the $4f$ energies. The advantage of presenting the data in terms of $4f$ energies is that these are directly related to the relative stability of the divalent and trivalent valence states, see Sec. IV.

The assumption that the $4f$ and $5p$ levels show the same chemical shift requires a comment. In those cases when the $4f$ and $5p$ energies can both be measured with good accuracy it is seen that the chemical shifts of these two levels agree well. However, for the pure Yb metal the $5p$ to $4f$ separation is 0.2 eV smaller than for the overlayer systems. This shows that the $5p$ levels undergo somewhat smaller shifts than the $4f$ levels. This can be

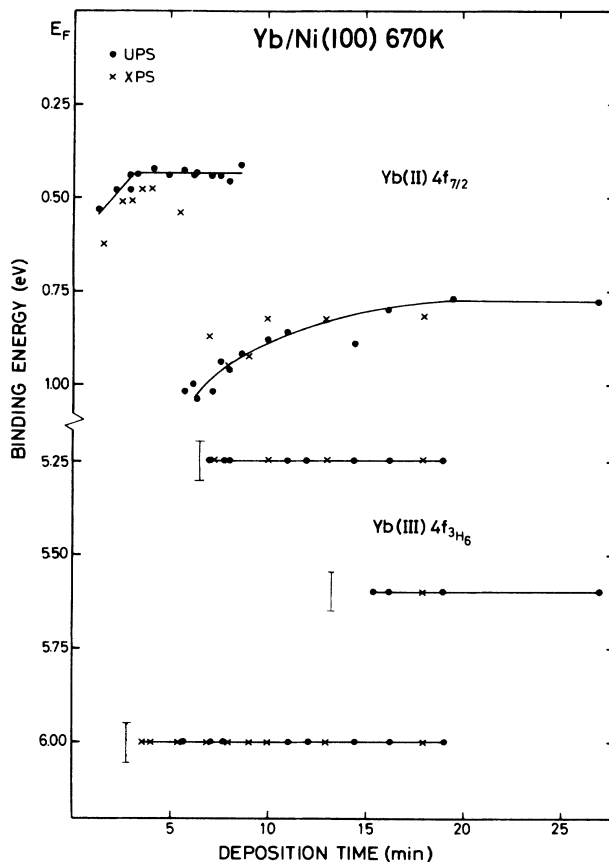


FIG. 10. Divalent and trivalent $4f$ binding energies as a function of deposition time for 670-K depositions. Error bars in the trivalent binding energies are indicated.

explained by the more extended character of the $5p$ orbitals. However, for the small shifts between different overlayer situations this effect will have only a minor influence.

Starting at low depositions of Yb we first of all note that it is rather complicated to extract detailed binding energies in this region due to the low Yb intensity. In XPS with its larger information depth the signal to background ratio for the weak overlayer peak becomes very low. In the UPS spectra one faces instead the problem of correctly taking into account the sloping background. However, by combining the XPS and UPS results a good picture of the development of the Yb binding energy has been obtained also in the low-coverage regime.

From the XPS spectra it is seen that the first deposited Yb becomes divalent. For 1.5-min deposition time a $4f$ binding energy of 0.55 eV is obtained. This binding energy is considerably lower than for Yb metal. The surface $4f$ peak position in Yb metal is 1.7 eV, see Fig. 8. Compared to this situation the presently observed surface feature has shifted by as much as 1.15 eV. This indicates a large coordination of the Yb atoms to Ni, i.e., to a large c_{Ni}^* . Also the reduction of $c_{\text{Yb}^{2+}}^*$ for Yb on Ni compared to Yb metal will give a shift contribution in the observed direction. The $5p_{3/2}$ line in UPS is relatively broad for this situation with a pronounced asymmetry towards

higher binding energies. This shows that there are more than one type of Yb atoms present at these coverages.

Increasing the deposition time to 2.5 min leads to a decrease of the $4f$ binding energy and a narrowing of the line. These two effects are due to the disappearance of the emission at the high-binding-energy side of the asymmetric peak, see Fig. 2. By further deposition the decrease in the binding energy continues and levels off at a $4f$ binding energy of 0.43 eV after 3.5-min deposition time. This shift first of all shows that the adsorption at low coverages is not dominated by the formation of large islands. In such a case a constant binding energy would be expected. The observed behavior instead suggests that the initial adsorption involves rather separated Yb atoms with a distribution of different sites. The shift is then due to an increasing adsorbate-adsorbate interaction as the density of the two-dimensional Yb film increases. This interaction forces all Yb atoms to populate more similar adsorption sites. Expressed in terms of the parameters in Eq. (7) we note that increasing the density of the overlayer film in an effective sense corresponds to increasing the value of c_Z^* and decreasing the value of c_V^* . The partial shifts ΔE_Z and ΔE_V are both positive, see Fig. 8, why these two effects will lead to shifts in different directions. However, since ΔE_V is considerably larger we expect this term to dominate. This means that a shift to lower binding energies is expected.

Similar types of shifts have previously been reported for the adsorption of K on Ru(001).⁴² Qualitatively the arguments above can be directly transferred to the case of a monovalent metallic adsorbate. This is due to the fact that the creation of a core hole in a monovalent and a divalent metal atom will change the properties of the ionized atom in the same direction. The cohesive forces will, for instance, in both cases tend to stabilize the final state over the initial state.

After 3.5-min deposition time we enter the second part of region 1. In this region an incommensurate overlayer structure is seen in LEED.²⁶ In Fig. 10 we notice two characteristic features in this region. Firstly, the binding energy of the divalent signal becomes constant. Secondly, a trivalent feature appears in the spectra at 6.0-eV binding energy. As seen in Fig. 9, this energy position for trivalent Yb is rather high. This suggests that the trivalent atoms are located at the surface. This is also supported by an analysis of the AES and ISS intensities.²⁶ In Fig. 9 the binding energy for the surface of a hypothetically trivalent Yb metal was derived to be 6.3 eV. The presently observed surface feature has a lower binding energy, which indicates that it can have a larger coordination than what would be obtained at the surface of the pure metal. The fact that divalent and trivalent Yb atoms are coexisting in the surface region may also give a positive shift of the trivalent $4f$ level, see Fig. 8. Taking also this effect into account we find that a binding energy of 6.0 eV may be obtained even for a rather complete coordination of the trivalent Yb site. It is, however, clear that this feature must be associated with the surface layer since it is only the reduced coordination at the surface or the direct interaction with the divalent Yb atoms which are located within the surface layer that can explain the

observed binding energy.

We notice that the divalent $4f$ binding energy is very low in this region. This means that the divalent site is rather close to becoming trivalent. The difference between the divalent and trivalent sites in this structure need therefore not be very large. In terms of Fig. 8 the divalent site corresponds to a $4f$ position close to but below the line of zero. Already a small increase in the coordination to Ni (increasing c_{Ni}^* and decreasing c_V^*) may then lead to a trivalent Yb site instead (corresponding to a negative binding energy in Fig. 8).

When the ring 1 pattern develops in region 1 there is a slight increase in the width of the divalent feature, see Fig. 2. This pattern has been interpreted as due to an incommensurate overlayer structure which implies that the Yb overlayer is out of registry with the substrate. In such a structure the Yb atoms will populate a large number of different adsorption sites, which explains the larger width of the $5p$ peak. From the appearance of trivalent intensity in this region it is furthermore seen that the difference between the sites is large enough to make a fraction of the Yb atoms trivalent.

After 6-min deposition time region 2 is entered. In this region a $c(10 \times 2)$ overlayer structure is observed.²⁶ In the spectra we observe some new features which can be associated with a change in the overlayer structure. In the divalent part of the spectrum we observe that a new component appears at 1.05 eV. Simultaneously a new trivalent feature at 5.2 eV binding energy appears which exists together with the previously observed feature at 6.0 eV.

The divalent $4f$ feature at 0.4 eV which is typical for the ring 1 structure gradually disappears in region 2 and at the end of the region where the $c(10 \times 2)$ structure is fully developed this feature is no longer seen. The coexistence of the spectra corresponding to the ring 1 and the $c(10 \times 2)$ structures in this region shows that the $c(10 \times 2)$ structure nucleates in islands. This is in agreement with LEED measurements which sometimes show the ring 1 and the $c(10 \times 2)$ structures simultaneously.

In the trivalent part of the spectrum we note that the 6.0-eV feature is a property also of the $c(10 \times 2)$ overlayer system. As for the ring 1 structure there are thus trivalent surface atoms present in the $c(10 \times 2)$ structure. The new trivalent feature at 5.2 eV, on the other hand, has a binding energy which is indicative of strongly coordinated bulk trivalent atoms. This implies that there is a real three-dimensional growth of the film in this region. This conclusion has also been drawn from the AES and ISS investigations.²⁶

We interpret the 5.2 eV position as due to an interface shift between a compound layer and the Ni substrate. As seen from Fig. 9 this energy is lower than the bulk binding energy in $YbNi_5$. In this compound Yb has only Ni nearest neighbors. However, the lower binding energy of the interface peak indicates that c_{Ni}^* is even larger for the interaction with a full Ni-metal layer than for the dilute compound.

Since all $YbNi_x$ compounds are trivalent in the bulk the divalent intensity also in region 2 has to be identified with surface atoms. As seen from Fig. 10 this divalent

feature is shifted by 0.6 eV to higher binding energies compared to region 1. According to Fig. 8 this can be explained by a lower total coordination of the divalent atoms (larger c_V^*) and/or by a lower coordination to Ni (smaller c_{Ni}^*). We noted above that this region corresponds to the formation of an intermetallic compound containing also bulk Yb atoms. In this way the Yb surface atoms are now located on top of an Yb-Ni compound layer, which leads to the required reduction of c_{Ni}^* . The observed shift therefore gives further evidence for the formation of a compound layer. In the trivalent surface signal no corresponding shift is seen. However, as seen from Fig. 9 an increase of c_{Ni}^* will have a much smaller effect on the trivalent $4f$ energy. Furthermore, the divalent and trivalent surface sites may also be different in terms of the coordination to Yb and Ni in the underlying layer.

In region 2 there is gradual decrease of the divalent Yb $4f$ binding energy by 0.15 eV. It was previously concluded that the $c(10 \times 2)$ structure nucleates in islands. This might explain such a shift. If the islands originally are rather small there will be a large fraction of atom at the edges of these islands. The Yb atoms at the edges will naturally have lower coordination (larger c_V^* and smaller c_{Ni}^*) than the atoms in the center of the islands. From Fig. 8 it is seen that such edge atoms would have a larger $4f$ binding energy.

When entering region 3 there is a gradual change of the spectrum to a new situation. For the fully developed Final structure the spectrum shows only one divalent and one trivalent component. The trivalent component has an energy which is intermediate between the two trivalent energies seen in region 2. XPS shows that this feature grows in intensity with continued deposition and is therefore identified with the bulk of the compound which is formed. The $4f$ energy in this region is 5.6 eV, which is identical to the observed position for bulk $YbNi_x$ compounds.³⁸ The much larger fraction of divalent Yb seen in UPS than in XPS also shows that the divalent Yb is located at the surface of the compound which is formed.

Some remarks on the development of the structures in the Yb/Ni(100) system can also be made using the observed variations in the divalent and trivalent $4f$ and $5p$ intensities. In Ref. 26 it was found that the area of the $c(10 \times 2)$ unit cell is six times larger than that of the unit cell of the Final structure. If we assume one Yb atom per unit cell in the final structure (the two-dimensional unit cell is too small to contain two Yb atoms), the $c(10 \times 2)$ unit cell contains six Yb atoms. The ratio of trivalent to divalent intensities was estimated to 3:2 in the $c(10 \times 2)$ structure, see Sec. III. Furthermore, in the XPS spectra it was seen that the intensity of the surface trivalent feature was significantly lower than the bulk counterpart. One possibility is then that there are two trivalent and four divalent sites per $c(10 \times 2)$ unit cell in the surface layer and four to six trivalent atoms in the underlying interface layer (it is difficult to estimate the escape depth influence of the bulk trivalent intensity). The $c(10 \times 2)$ structure would in this way be a true unit cell and not a coincidence cell with the underlying Ni(100) substrate.

In the final structure the divalent intensity has increased by roughly 50%. This could be understood as a rearrangement of the surface layer in the $c(10 \times 2)$ structure, generating the same type of divalent site for all the surface Yb atoms. This would lead to the observed smaller unit cell containing only one Yb atoms.

The large width of the divalent $5p_{3/2}$ peak in the $c(10 \times 2)$ structure, see Fig. 2 further indicates that there are several different divalent sites in the surface layer. This is consistent with the model proposed above, which allows for four divalent sites per $c(10 \times 2)$ unit cell. When the final structure develops the divalent peak narrows and shifts by 0.1 eV to lower binding energy. It is in particular the high-binding-energy components that disappears. This is consistent with the formation of a structure in which there is only one type of divalent Yb present.

For a number of lanthanide overlayer systems the possibility of homogeneous mixed valent has been discussed.⁴³⁻⁴⁵ However, in these studies the possibility of intermixing with the substrate has not been considered. Based on the $4f$ binding energies some conclusions about the possibility that a mixed-valent situation is homogeneous can be drawn. A necessary condition for homogeneous mixed valence to occur is that the divalent $4f$ level is located in the vicinity of the Fermi level (corresponding to an energy degeneracy of the divalent and trivalent configurations). This criterium is difficult to quantify in detail^{27,46} However, it is clear that the $c(10 \times 2)$ situation is heterogeneously mixed valent.²⁷ We also consider the ring 1 structure to be heterogeneously mixed valent, although the $4f$ binding energy is only slightly larger than 0.4 eV in this region which is becoming rather close to a binding energy which could possibly be consistent with a homogeneously mixed-valent situation. Evidence that this situation is heterogeneously mixed valent is also obtained from the $5p$ core-level widths in Fig. 2. As discussed above, there is a slight broadening of the spectrum for the ring 1 structure, which indicates that different adsorption sites are populated. The same conclusion is also obtained by LEED which shows that this structure is incommensurate with the Ni(100) substrate. In this situation it is most reasonable to assume that the appearance of both divalent and trivalent features in the spectrum is due to different adsorption sites.

B. Binding energies—room temperature

The Yb spectral features are generally broader when recorded at room temperature (RT) than at 670 K. This shows that a number of different Yb sites are populated, which implies a low mobility of the Yb atoms at this temperature. The RT overlayers are thus structurally less well defined than the ones formed at 670 K. This is also seen from the fact that no ordered overlayer LEED patterns are seen for the RT depositions. The appearance of LEED patterns requires annealing of the deposited films. Due to the broader spectral features and the varying widths of the peaks we have not summarized the measured binding energies in a diagram as was done for the 670-K depositions. However, there are still several con-

clusions that can be drawn from the observed binding energies.

At low coverages the spectra are very similar to the ones obtained at 670 K. For short deposition times only divalent spectra features are seen. As for the 670-K situation we interpret these spectra as due to adsorbed Yb atoms with a distribution of differently coordinated sites.

After 3-min deposition time also a trivalent component appears in the $4f$ spectra. This component has the same binding energy (6.0 eV) as the trivalent feature observed for similar coverages at 670 K. From the binding energy it is concluded that this feature is due to surface trivalent atoms, see the discussion of the 670-K spectra. It seems that the trivalent component appears at somewhat lower coverages at room temperature than at 670 K. It is also seen that the divalent spectrum is broader than at 670 K and that the peaks are asymmetric towards higher binding energies. These observations indicate that there is a distribution of local arrangements at the surface. This can be explained by the reduced mobility of the Yb atoms at RT. Due to local variations in the Yb overlayer density a number of different situations which were connected to different deposition times at 670 K are therefore experienced simultaneously.

The XPS spectrum obtained after 12-min deposition time is rather similar to the 5-min spectrum. This is completely different from the situation at 670 K. In that case a surface layer of an intermetallic compound [connected to the $c(10 \times 2)$ structure] was formed for such deposition times, which resulted in major effects in the spectra. The 12-min situation at RT is instead interpreted as due to Yb atoms located on top of the Ni(100) surface. The sites which are populated are very different with at least two distinctly different types of sites as seen from the occurrence of both divalent and trivalent Yb atoms.

In the spectrum obtained after 19-min deposition time some major changes are seen. The trivalent $4f$ component is shifted to a lower binding energy (5.4 eV) and the divalent component is shifted by 0.1 eV towards larger binding energies. The large shift (0.6 eV) of the trivalent peaks indicates that the Yb^{3+} atoms are now located in the bulk, see Fig. 9. One possibility to explain the occurrence of bulk trivalent Yb is that there is a weak intermixing at the interface with the formation of a disordered bulk compound. The observed trivalent $4f$ binding energy seems to be too low for any existing YbNi_x compound, see Fig. 9. However, for Yb atoms located very close to the unreacted Ni substrate it seems that the binding energy could be lower, see the discussion of the $c(10 \times 2)$ structure above.

As an alternative explanation it is seen from Figs. 8 and 9 that the growth of a second Yb layer on top of the first layer could produce the observed spectrum with a trivalent component at the right energy position due to the interface layer. In such a case the divalent signal originates from the surface on top of this interface. At first we consider the stability difference between the divalent and trivalent configurations for the interface layer. As seen from Fig. 8 already a relatively small c_{Ni}^* is sufficient to stabilize the trivalent configuration. From

Fig. 9 it can then be concluded that the trivalent binding energy at this interface would be rather close to the position which is marked for the interface between an Yb-Ni overlayer and the Ni substrate (upper dashed line). Compared to this situation, the only major shift contribution is due to the interaction with the divalent Yb atoms in the surface layer. According to the figure this will produce a shift to higher binding energies which is exactly as observed.

The simultaneous increase of the divalent binding energy could be explained by the difference between a monolayer on top of a Ni substrate or on top of a trivalent Yb layer. The partial shifts due to Ni and trivalent Yb neighbors have the same sign but the shift due to Ni neighbors is considerably larger, see Fig. 8. A reduced number of Ni neighbors, even if compensated by an increased number of trivalent Yb neighbors, would therefore lead to an increase in the Yb^{2+} binding energy.

From the discussion above it is clear that a deposition of 19 min must be well above one monolayer of Yb, whereas 12 min seems to be within the range of completing the first monolayer. This approximate location of the monolayer point is supported by the AES growth curves and the ISS spectra.²⁶

Turning to larger coverages, it is seen that the divalent binding energy continues to increase with deposition time until the pure Yb metal spectrum is observed. At deposition times much larger than 50 min the trivalent feature is still observable. This indicates a Stranski-Krastanov growth mode with the formation of large three-dimensional islands. The large surface core-level shift for the thick film indicates the existence of many Yb surface sites with a low coordination number in this film.³⁰

VII. SUMMARY AND CONCLUSIONS

In the present paper we have investigated Yb overlayers on Ni(100) by XPS and UPS. The $4f$ binding energies of divalent and trivalent Yb have been treated within a model for core-level shifts in Lanthanide overlayer systems. Valuable structural information can be obtained by a careful analysis of the binding energies and the half widths of the Yb spectral features.

For the 670-K depositions, the initial adsorption is interpreted as due to separated divalent Yb atoms with a distribution of adsorption sites. For larger coverages an incommensurate structure develops with a distribution of divalent and trivalent sites. With further deposition an intermixing with the substrate takes place leading to a $c(10 \times 2)$ structure. This large unit cell contains four divalent sites, at least some of which are inequivalent, and two trivalent sites in the surface layer. There are four to six trivalent Yb atoms in the underlying interface layer towards the Ni(100) substrate. When the compound thickens a slightly distorted hexagonal structure develops with one divalent site in the surface layer and one type of trivalent sites in the bulk. The binding energy of the trivalent feature agrees well with the measured $4f$ position in bulk YbNi_x compounds.

No ordered structures are observed for room tempera-

ture depositions. The spectral features are generally broader than for the 670-K depositions. No strong intermixing with the substrate is observed. Instead a layer growth mode seems to be favored up to two monolayers. At larger Yb doses divalent Yb grows in a Stranski-Krastanov growth mode. The interface layer towards the substrate becomes trivalent when the second layer starts to grow.

ACKNOWLEDGMENTS

The assistance of J. O. Forsell and H. Rydåker is gratefully acknowledged. This work was supported by the Danish and Swedish Natural Science Research Councils and the Swedish Board for Technical Development. Travel support was provided by the Nordic Council.

*Present address: MAX-laboratory, University of Lund, Box 118, S-221 00 Lund, Sweden.

¹K. Siegbahn, C. Nordling, A. Fahlman, R. Nordberg, K. Hamrin, J. Hedman, G. Johansson, T. Bergmark, S. E. Karlsson, I. Lindgren, and B. Lindberg, *ESCA-Atomic, Molecular and Solid State Structure Studied by Means of Electron Spectroscopy*, (North-Holland, Amsterdam, 1967).

²K. Siegbahn, C. Nordling, G. Johansson, J. Hedman, P. F. Heden, K. Hamrin, U. Gelius, T. Bergmark, L. O. Werme, R. Manne, and Y. Baer, *ESCA Applied to Free Molecules* (North-Holland, Amsterdam, 1969).

³D. A. Shirley, *J. Electron. Spectrosc. Relat. Phenom.* **5**, 135 (1974).

⁴H. Basch, *J. Electron. Spectrosc. Rel. Phen.* **5**, 463 (1974).

⁵J. F. Herbst, D. N. Lowy, and R. E. Watson, *Phys. Rev. B* **6**, 1913 (1972).

⁶D. A. Shirley, R. L. Martin, S. P. Kowalczyk, F. R. McFeely, and L. Ley, *Phys. Rev. B* **15**, 544 (1977).

⁷A. R. Williams and N. D. Lang, *Phys. Rev. Lett.* **40**, 954 (1978).

⁸B. Johansson and N. Mårtensson, *Phys. Rev. B* **21**, 4427 (1980).

⁹P. Steiner, S. Hüfner, N. Mårtensson, and B. Johansson, *Solid State Commun.* **37**, 73 (1981).

¹⁰P. Steiner and S. Hüfner, *Solid State Commun.* **37**, 79 (1981).

¹¹N. Mårtensson, R. Nyholm, H. Calen, J. Hedman, and B. Johansson, *Phys. Rev. B* **24**, 1725 (1981).

¹²A. Rosengren and B. Johansson, *Phys. Rev. B* **22**, 3706 (1980).

¹³B. Johansson and N. Mårtensson, *Helv. Phys. Acta* **56**, 405 (1983).

¹⁴D. Spanjaard, C. Guillot, M. C. Desjonqueres, G. Treglia, and J. Lecante, *Surf. Sci. Rep.* **5**, 1 (1985).

¹⁵M. Domke, T. Mandel, C. Laubschat, M. Prietsch, and G. Kaindl, *Surf. Sci.* **189/190**, 268 (1987).

¹⁶N. Mårtensson, A. Stenborg, O. Björneholm, A. Nilsson, and J. N. Andersen, *Phys. Rev. Lett.* **60**, 1731 (1988).

¹⁷A. Nilsson, N. Mårtensson, J. Hedman, B. Eriksson, R. Bergman, and U. Gelius, *Surf. Sci.* **162**, 51 (1985).

¹⁸D. Chadwick and M. A. Karolewski, *Surf. Sci.* **126**, 41 (1983).

¹⁹A. Fujimori, M. Grioni, and J. H. Weaver, *Phys. Rev. B* **33**, 726 (1986).

²⁰K. Gürtler and K. Jacobi, *Surf. Sci.* **134**, 309 (1983).

²¹C. Somerton, C. F. McConville, D. P. Woodruff, and R. G. Jones, *Surf. Sci.* **136**, 23 (1984).

²²P. Steiner and S. Hüfner, *Solid State Commun.* **37**, 279 (1981).

²³S. B. DiCenzo, G. K. Wertheim, and D. N. E. Buchanan, *Phys. Rev. B* **30**, 553 (1984).

Phys. Rev. B **30**, 553 (1984).

²⁴*Handbook on the Physics and Chemistry of Rare Earths, Volume 10: High Energy Spectroscopy*, edited by K. A. Gschneidner, Jr., L. Eyring, and S. Hüfner (North-Holland, Amsterdam, 1987).

²⁵J. N. Andersen, J. Onsgaard, A. Nilsson, B. Eriksson, E. Zdansky, and N. Mårtensson, *Surf. Sci.* **189/190**, 399 (1987).

²⁶J. N. Andersen, J. Onsgaard, A. Nilsson, B. Eriksson, and N. Mårtensson, *Surf. Sci.* **202**, 183 (1988).

²⁷A. Nilsson, B. Eriksson, N. Mårtensson, J. N. Andersen, and J. Onsgaard, *Phys. Rev. B* **36**, 9308 (1987).

²⁸S. M. Goldberg, C. S. Fadley, and S. Kono, *J. Electron Spectrosc. Relat. Phenom.* **21**, 285 (1981).

²⁹M. H. Hecht, A. J. Viescas, I. Lindau, J. W. Allen, and L. I. Johansson, *J. Electron Spectrosc. Relat. Phenom.* **34**, 343 (1984).

³⁰W.-D. Schneider, C. Laubschat, and B. Reihl, *Phys. Rev. B* **27**, 6538 (1983).

³¹W. T. Carnall, P. R. Fields, and K. Rajnak, *J. Chem. Phys.* **49**, 4424 (1968).

³²The intensities of the multiplet lines are varied to obtain the best fit. It should, however, be noted that this fit is not unique.

³³A. R. Miedema, *J. Less-Common Met.* **32**, 117 (1973).

³⁴A. R. Miedema and P. F. Chatel, in *Proceedings of the Symposium at the 108th AIME Annual Meeting, New Orleans 1979* (unpublished).

³⁵N. Mårtensson and M. Neumann (unpublished).

³⁶B. Johansson and P. Munck, *J. Less-Common Metals* **100**, 49 (1985).

³⁷A. Palenzona and S. Cirafici, *J. Less-Common Metals* **33**, 361 (1973).

³⁸G. K. Wertheim, J. H. Wernick, and G. Creelius *Phys. Rev. B* **18** 875 (1978).

³⁹B. Johansson, *Phys. Rev. B* **20**, 1315 (1979).

⁴⁰J. K. Lang, Y. Baer, and P. A. Cox, *J. Phys. F* **11**, 121 (1981).

⁴¹F. Gerken, A. S. Flodström, J. Barth, L. I. Johansson, and C. Kunz, *Phys. Scr.* **32**, 43 (1985).

⁴²J. J. Weimer, E. Umbach, and D. Menzel, *Surf. Sci.* **159**, 83 (1985).

⁴³Å. Fäldt and H. P. Myers, *Phys. Rev. Lett.* **52**, 1315 (1984).

⁴⁴Å. Fäldt and H. P. Myers, *Phys. Rev. B* **30**, 5481 (1984).

⁴⁵Å. Fäldt and H. P. Myers, *Phys. Rev. B* **34**, 6675 (1986).

⁴⁶J. N. Andersen, I. Chorkendorff, J. Onsgaard, J. Ghijsen, R. L. Johnson, and F. Grey, *Phys. Rev. B* **37**, 4809 (1988).